AGU PUBLICATIONS

Geochemistry, Geophysics, Geosystems

RESEARCH ARTICLE
10.1002/2016GC006734

Key Points:
- A full eruption cycle at Axial seamount was captured by a network of seafloor hydrophones
- Signals recorded by seafloor hydrophones represent different eruptive mechanisms
- A signal interpreted as Hawaiian-style explosive degassing and ash generation is identifiable in hydroacoustic data

Correspondence to:
J. Caplan-Auerbach,
caplanj@wwu.edu

Citation:
Caplan-Auerbach, J., R. P. Dziak, J. Haxel, D. R. Bohnenstiehl, and C. Garcia (2017), Explosive processes during the 2015 eruption of Axial Seamount, as recorded by seafloor hydrophones, *Geochem. Geophys. Geosyst.*, *18*, 1761–1774, doi:10.1002/2016GC006734.

Received 15 NOV 2016
Accepted 3 APR 2017
Accepted article online 12 APR 2017
Published online 26 APR 2017

Explosive processes during the 2015 eruption of Axial Seamount, as recorded by seafloor hydrophones

J. Caplan-Auerbach[1], R. P. Dziak[2], J. Haxel[2,3], D. R. Bohnenstiehl[4], and C. Garcia[5]

[1]Department of Geology, Western Washington University, Bellingham, Washington, USA, [2]NOAA/Pacific Marine Environmental Laboratory, Newport, Oregon, USA, [3]Cooperative Institute for Marine Resources Studies, Oregon State University, Newport, Oregon, USA, [4]Department of Marine, Earth and Atmospheric Sciences, North Carolina State University, Raleigh, North Carolina, USA, [5]School of Oceanography, University of Washington, Seattle, Washington, USA

Abstract Following the installation of the Ocean Observatories Initiative cabled array, the 2015 eruption of Axial Seamount, Juan de Fuca ridge, became the first submarine eruption to be captured in real time by seafloor seismic and acoustic instruments. This eruption also marked the first instance where the entire eruption cycle of a submarine volcano, from the previous eruption in 2011 to the end of the month-long 2015 event, was monitored continuously using autonomous ocean bottom hydrophones. Impulsive sounds associated with explosive lava-water interactions are identified within hydrophone records during both eruptions. Explosions within the caldera are acoustically distinguishable from those occurring in association with north rift lava flows erupting in 2015. Acoustic data also record a series of broadband diffuse events, occurring in the waning phase of the eruption, and are interpreted as submarine Hawaiian explosions. This transition from gas-poor to gas-rich eruptive activity coincides with an increase in water temperature within the caldera and with a decrease in the rate of deflation. The last recorded diffuse events coincide with the end of the eruption, represented by the onset of inflation. All the observed explosion signals couple strongly into the water column, and only weakly into the solid Earth, demonstrating the importance of hydroacoustic observations as a complement to seismic and geodetic studies of submarine eruptions.

Plain Language Summary Axial Seamount, a submarine volcano on the Juan de Fuca ridge, erupted in 2015. This eruption was recorded in real-time by an array of seafloor seismometers and hydrophones located on the volcano, and connected to shore by a power and data cable. Hydrophones recording the sounds generated by the eruption reveal several different types of explosions, including short bursts interpreted as lava-water interactions, and prolonged signals thought to be due to explosive ejection of gas and ash. These signals provide a window into the dynamics of the undersea eruption and are an excellent complement to other types of data including earthquakes and ground deformation.

1. Introduction

Approximately 80% of Earth's volcanic productivity occurs beneath the ocean where it is extremely difficult to monitor and observe eruptive activity. Only two submarine volcanoes have ever been observed in active eruption: NW Rota-1 volcano in the Marianas [*Embley et al.*, 2006] and West Mata volcano in the Tonga arc [*Resing et al.*, 2011]. Eruptions of two others, Axial Seamount on the Juan de Fuca ridge in 1998 and 2011 [*Dziak and Fox*, 1999; *Chadwick et al.*, 2012] and the 9°50'N section of the East Pacific Rise [*Tolstoy et al.*, 2006; *Tan et al.*, 2016], were captured by in situ instrumentation but not directly observed. Eruptions at the Gakkel Ridge were observed in 1999 [*Müller and Jokat*, 2000; *Tolstoy et al.*, 2001] by the global seismic network and again in 2001 [*Schlindwein et al.*, 2005] by a local network of seismometers attached to an ice flow. Although T-phase recordings on Navy hydrophone arrays provided real-time observation of eruptions on the Gorda and Juan de Fuca ridges, no in situ data were available [*Fox et al.*, 1995; *Fox and Dziak*, 1998; *Rubin et al.*, 2012].

In April 2015, Axial Seamount again erupted, depositing 1.48×10^8 m^3 of basaltic lava within the caldera and on the volcano's north rift [*Chadwick et al.*, 2016]. For at least two reasons, this event was unique among submarine eruptions: (1) it was monitored in real time by instruments deployed on and near the volcano as part of the Ocean Observatories Initiative (OOI) cabled observatory and (2) the complete eruptive cycle was

recorded by temporary networks of autonomous seafloor hydrophones deployed by NOAA over a period nearly a decade [*Dziak et al.*, 2012]. The combination of real-time and long-term instrumentation [*Dziak et al.*, 2012] provides the only complete and continuous record of seismic and explosive activity over a full eruption cycle on a submarine volcano.

The seismicity and deformation of the 2015 eruption has been described by *Wilcock et al.* [2016] and *Nooner and Chadwick* [2016]. This paper complements those studies by examining earthquake and explosion signals associated with the 2011 and 2015 eruptions, as recorded by seafloor hydrophones. We present acoustic signals interpreted as eruption sounds, including lava-water interactions in Axial's caldera and on the north rift. Moreover, we introduce a new category of acoustic signal, a prolonged broadband signal that we interpret as submarine Hawaiian explosive activity. These hydroacoustic data provide a unique perspective that spans the two eruptions and both complements and enhances the seismic and deformation data presented by *Wilcock et al.* [2016] and *Nooner and Chadwick* [2016].

2. Axial Seamount

Axial Seamount is the youngest expression of the Cobb hot spot and is colocated with the Juan de Fuca ridge, approximately 475 km west of the Oregon coast (Figure 1). The volcano has a 3 km × 8 km summit caldera and elongate rift zones extending both north and south along the Juan de Fuca ridge [*Embley et al.*, 1990;

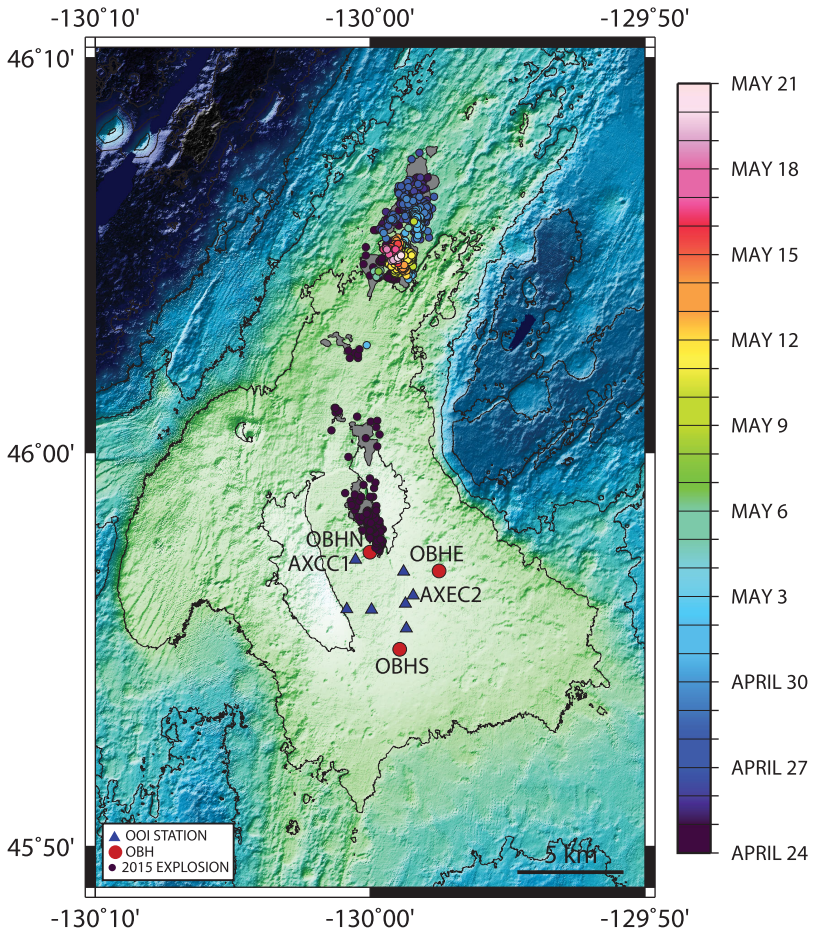

Figure 1. Map of Axial caldera, Juan de Fuca ridge. Blue triangles represent stations in the cabled array of the Ocean Observatories Initiative (OOI), while the red circles are seafloor hydrophones deployed by NOAA; only stations mentioned in the text are named here. OOI stations AXCC1 and AXEC2 are broadband seismic stations with colocated ocean-bottom hydrophones. An additional broadband OOI station AXBA1 (not shown here) lies ~25 km southeast of the caldera. The gray shapes represent deposits from the 2015 eruption, as identified by bathymetric difference mapping (flow outlines courtesy S. Merle, NOAA/HMSC). Colored circles are locations of 2015 explosion signals detected by stations of the OOI network, color coded by occurrence time.

Clague et al., 2013]. Seismoacoustic data suggest that during its eruptions magma can propagate up to 50 km from the caldera [*Dziak and Fox*, 1999].

Acoustic monitoring of activity at Axial began in 1991 when scientists were given access to the US Navy's SOund Surveillance System (SOSUS) hydrophones [*Dziak and Fox*, 1999]. Three eruptions have occurred at Axial since that time, in 1998, 2011, and 2015, and these eruptions have been recorded by a variety of in situ instruments including bottom pressure sensors [*Fox*, 1999; *Fox et al.*, 2001; *Chadwick et al.*, 2006; *Nooner and Chadwick*, 2009; *Chadwick et al.*, 2012; *Nooner and Chadwick*, 2016] and ocean-bottom hydrophones [*Dziak and Fox*, 1999; *Sohn et al.*, 1999; *Dziak et al.*, 2012]. Geophysical signals recorded during the eruptions include caldera subsidence, seismic activity, and thermal changes [*Fox et al.*, 2001; *Chadwick et al.*, 2006, 2012; *Dziak et al.*, 2012]. Ocean-bottom hydrophones (OBHs) deployed on Axial recorded earthquakes, tremor, and explosions associated with the 2011 eruptive activity [*Dziak et al.*, 2012]. These acoustic data were of critical importance in determining the rate of dike propagation from the caldera to the south rift [*Dziak et al.*, 2012].

While instrumental data recorded in 1998 and 2011 were crucial to interpreting the progress of those eruptions, the data were not available in real-time, and thus analysis of the events was performed well after the eruptive activity had ended. The 2015 eruption, however, occurred shortly after the deployment of the Ocean Observatory Initiative array of cabled instruments (OOI) [*Kelley et al.*, 2014]. The Axial array includes seven three-component seismometers (two broadband, five short period) deployed along the summit of the volcano, with both broadband sensors being colocated with an ocean-bottom hydrophone (Figure 1). There is an additional eighth station, containing a broadband seismometer and hydrophone, deployed at the base of the volcano, ~25 km to the southeast of the summit array. All of these stations send data in real time to a shore station in Pacific City, Oregon. This makes the 2015 Axial eruption the first submarine eruption to be monitored with in situ data in real time from the precursory sequence to the end of the eruption.

3. The Long-Term Hydroacoustic Record

Semiannual deployments of one to three NOAA ocean-bottom hydrophones within and near the caldera (Figure 1) provided a continuous view of seismic and acoustic activity at Axial from 2006 until July 2015 (Figure 2) [*Dziak et al.*, 2012]. Microearthquake data processing of the OBH data utilizes an automated detection algorithm [*Mellinger*, 2001] tuned for low-frequency hydroacoustic earthquake energy that is applied to the raw hydrophone record. Detection of an earthquake arrival is triggered when the summation of spectral energy in the 0.1 Hz $< f <$ 10 Hz band calculated from a 1 s data block exceeds the energy summed over an 8 s window by a factor of 2. Events are then filtered by visual inspection to a subset of seismicity based on the sharp onset of *P* and inverted ocean surface reflected arrivals occurring at ~2 s spacing that are unique to locally generated microearthquakes at Axial Seamount [*Sohn et al.*, 2004]. Emergent seismic arrivals (*T*-phases) associated with more distant events are excluded. This method allows events to be counted based on data from a single station.

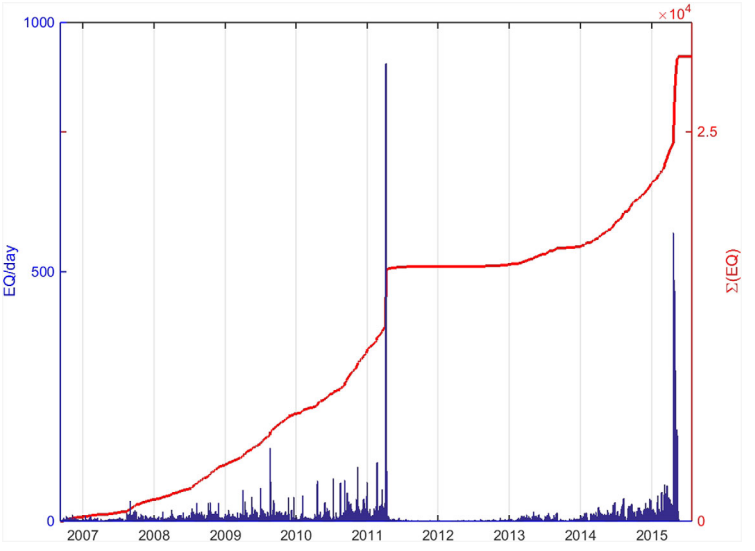

Figure 2. Histogram of signals detected by ocean-bottom hydrophones that were deployed and recovered semiannually by NOAA during an approximately 9 year period (2006–2015). The red line represents the cumulative number of earthquakes recorded during the ~9 year period. The peaks in activity in 2011 and 2015 are the two eruptions.

In general, both the 2011 and 2015 eruptions were preceded by a gradual (years) increase in seismicity with occasional swarms of >50 events per day, although

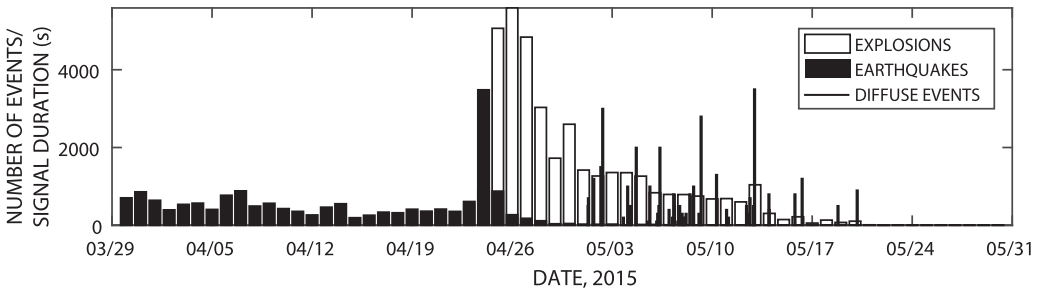

Figure 3. Daily histogram of earthquakes (black) and explosions (white) as recorded by hydrophones in the OOI cabled network during the 2015 eruption. Also plotted in narrow lines are the durations, in seconds, of 45 "diffuse events," interpreted here as prolonged explosive degassing, or Hawaiian eruptions.

changes in hydrophone location in 2011 and 2013 precludes a direct comparison of event numbers. The onsets of both eruptions were accompanied by a rapid increase in the number of signals recorded acoustically, with hundreds of events recorded daily during the eruptive periods. In the case of the 2011 eruption, hydroacoustic activity remained elevated for ~7 days, after which activity dropped to fewer than 10 daily events.

Between 2011 and 2015, the lowest level of local earthquake activity recorded by the OBH network took place between mid-July 2011 and August 2012, during which time an event was recorded once every 10 days on average (Figure 2). Activity began to increase again in November 2012, averaging just over one event per day through February 2013, and then increasing to an average of nearly five events per day through September 2013. There was a slight lull in activity between September 2013 and January 2014, when the network detected approximately two events per day.

In January 2014, the rate of local earthquake activity detected by the OBHs increased again, this time increasing continuously until the April 2015 eruption. During the onset of the eruption, the southern OBH (OBHS; Figure 1) detected 300–500 events per day. Because the OBH was located on the south rift, fairly far from where the lava flow eventually emerged in the eastern caldera, it recorded many times fewer events than were detected by OOI hydrophones (Figures 2 and 3). Acoustic data from both the OOI instruments and the OBH, as well as OOI deflation data and noncabled bottom pressure recorders, suggest that that eruption lasted approximately a month (Figure 2) [*Wilcock et al*., 2016; *Nooner and Chadwick*, 2016].

4. Overview of the 2015 Axial Eruption

Both the 2011 and 2015 eruptions initiated in the Axial caldera, with lava flows emanating from the central eastern caldera wall [*Chadwick et al*., 2012, 2016]. The 2015 eruption, however, rapidly transitioned to the north rift, where fresh lava was observed by bathymetric difference mapping [*Chadwick et al*., 2016]. The 2015 eruption was both longer in duration (1 month relative to the ~7 days of earthquake activity in 2011) and had a greater eruptive volume: the volume of material extruded in 2011 was estimated to be 1×10^8 m^3, whereas lava flows in 2015 had a volume of 1.48×10^8 m^3 [*Chadwick et al*., 2012, 2016]. In addition to lobate lava flows, deposits from the 2015 eruption include a layer of fine ash, collected from a benchmark in the central caldera.

Event counts for the 2015 eruption were performed differently for events identified as earthquakes and as explosions. Local microearthquakes were detected using a STA/LTA procedure operating on the band-passed (7–50 Hz) vertical channel waveforms. In-water sources (whale calls and explosions) were then screened based on the coherence between channels and spectral amplitude ratios. Explosions, in contrast, were counted using a match filtering technique. A set of ~800 isolated explosions, from times spanning the eruption, were selected as template events. A four-channel (the three-component seismometer and hydrophone) template matching routine was used to identify arrivals on station AXEC2, resulting in a set of 36,893 detections (correlation coefficient >0.7). For a subset of these detections, up to three arriving phases (bounces) were manually identified on stations across the caldera array. Locations were determined using a grid search routine that minimizes the RMS misfit to the arrival times, assuming a constant water depth of 1600 m and uniform sound velocity of 1.5 km/s.

High rates of seismicity (>100 events per day) at Axial were recorded from the beginning of the OOI installation (November 2014) [*Wilcock et al.*, 2016], with a gradual increase in activity beginning in March 2015 (Figure 3). Near 0420 UTC on 24 April 2015, a dramatic increase in seismic activity occurred, with rapid deflation beginning at ~0600, together marking what is assumed to be the beginning of the eruption (Figure 3) [*Wilcock et al.*, 2016; *Nooner and Chadwick*, 2016]. Seismic signals detected by the OOI seismic network had their origin within or near the caldera, near both the eastern and western caldera rims [*Wilcock et al.*, 2016]. Beginning on 25 April, however, a new category of signal was detected, originating from the north rift zones [*Garcia et al.*, 2015; *Wilcock et al.*, 2016]. These signals are interpreted as explosions on the seafloor, associated with the emplacement of lava flows and are discussed in more detail below.

5. Identification of Earthquake and Explosion Signals

P wave arrivals from local earthquakes beneath the caldera are recorded by both ocean-bottom hydrophone and vertical component seismic instrumentation. Upgoing seismic energy couples into the water column at the seafloor and is then reflected downward at the sea surface, producing a series of acoustic reverberations. Because the caldera floor lies at a depth of ~1500 m, these waterborne reverberations arrive at ~2 s intervals. Given the polarity convention of the OOI instrumentation, the sign of first arriving upgoing *P* waves energy is inverted between the hydrophone and vertical seismic channels, whereas downward propagating reverberations in the water column exhibit consistent polarity between sensors (Figure 4a) [*Hoffe et al.*, 1999; *Thorwart and Dahm*, 2005]. Because the hydrophone is omnidirectional, compressional waves generate a downward first motion regardless of whether the arrival comes from below ground or through the water column.

The north rift events are easily distinguished from subsurface earthquakes based on their arrival pattern and the consistent polarity observed between the hydrophone and vertical seismic channel (Figure 4b) [*Hoffe et al.*, 1999]. These signals couple strongly into the water column and are not observed to produce seismic body wave arrivals on the OOI network. The arrival pattern represents a series of multiple reflections

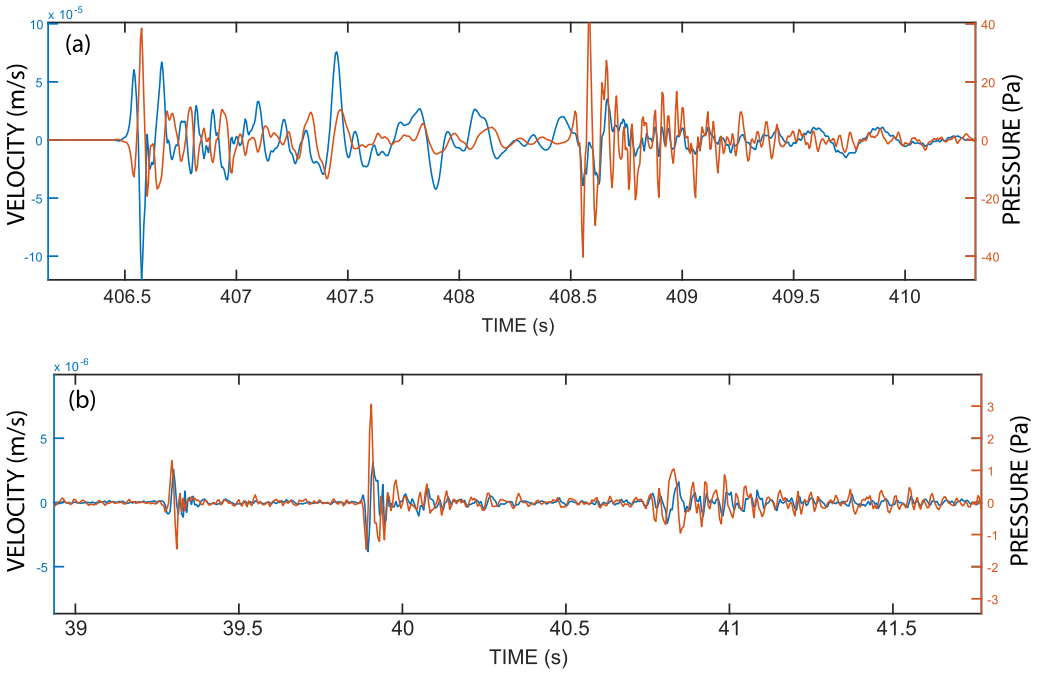

Figure 4. Example of a local (a) earthquake and (b) explosion, as recorded by the hydrophone (H, red) and vertical component seismometer (Z, blue) at OOI station AXCC1 on Axial Volcano. For the earthquake, signal polarity is reversed between the H and Z channels for *P* wave arrivals, consistent with an upward propagating signal. For the second phase, a sea surface reflection arriving 2 s later, the signal polarity is in-phase between channels, indicating a wave propagating downward through water column. An explosion, however, produces a series of water column multiples, each of which exhibits consistent polarity between the H and Z channels. Explosions time series are offset between channels by approximately one sample, consistent with the slower speed of hydroacoustic waves.

between the sea surface and seafloor, with the arrival delay time between bounces decreasing as a function of range between the source and receiver [*Dziak et al*., 2012; *Tan et al*., 2016].

Although the seismometer and hydrophones are considered to be collocated within the Axial network, the instruments are actually positioned several meters apart. Energy arriving from subsurface events arrives coincidentally on the seismometer and hydrophone while arrivals sourced in the water column arrive <1 sample (or 0.005 s) later on one of the instruments. This is due to the slower propagation of waves within the water relative to the subsurface, and it provides additional means by which events having a subsurface origin (earthquakes) may be distinguished from those originating in the water column (eruptive signals).

We agree with the interpretation of *Wilcock et al*. [2016] that the north rift signals are due to lava-water interactions. This interpretation is supported by the observation that there is no distinct seismic phase associated with these signals; seismic and acoustic signals are recorded simultaneously (within one sample), indicating that the signal was sourced within the water column and couples into the ground at the instrument. Whether the signal is explosive or implosive is more difficult to establish, as first motions are not clearly resolved: most signals have a low-amplitude emergent onset. Furthermore, north rift events have likely undergone a phase inversion due to a surface reflection. In this study we refer to the events as explosions but recognize that the generation of sound could also be due to an implosive source mechanism.

6. Three Types of Explosion Signals

Three categories of explosion signals were recorded by hydrophones during the 2015 eruption: (1) small impulsive events located close to the OOI hydrophones, (2) stronger impulsive signals colocated with the north rift lava flows, and (3) prolonged broadband signals interpreted as submarine Hawaiian ash eruptions (Figure 5). Both types of discrete explosion events include clusters that exhibit waveform similarity, which allowed us to extract event multiplets for analysis.

6.1. Caldera Explosions

The seismoacoustic signals located in or near the caldera are identifiable as explosions largely due to waveform polarity, because their surface reflections arrive at station AXCC1 between 1.5 and 1.9 s after the primary arrival (Figures 5 and 6b). Reflected arrivals at station AXEC2 arrive 1.3–1.7 s after the first pulse. Assuming that this represents the difference between a direct arrival and one reflected off of the sea surface, and assuming a speed of sound in water of 1480 m/s, this yields a source location of $\sim$400 m from OOI station AXCC1, and $\sim$1.5 km from AXEC2 (Figure 1), a location consistent with the caldera lava flow.

That the caldera signals are associated with a lava flow is supported by data from the 2011 eruption. At the time of that eruption, three OBHs were deployed near or within the caldera, although one station was destroyed by the lava flow. OBHE, the station located nearest the 2011 lava flow (Figure 1), recorded a subset of events with surface reflections occurring $\sim$2 s after the first arrival, consistent with a location near OBHE. Those same events recorded on OBHN (Figure 1) exhibit 1.5–2 s reflection timing (Figure 6a). This suggests a location very close to station OBHE and several hundred meters from the northern station, consistent with the location of the 2011 lava flow on the upper south rift zone [*Caress et al*., 2012].

6.2. North Rift Explosions

When compared to the caldera events, the north rift explosions are considerably stronger in amplitude, their secondary phases arrive $\sim$0.6 s after the primary arrival, and they have several additional phases that follow (Figures 4–6c). Analysis of reflection timing shows that their source locations coincide with areas where fresh lava flows were observed on Axial's north rift zone (Figure 1) [*Garcia et al*., 2015; *Chadwick et al*., 2016]. These events comprise the vast majority of explosive signals, with tens of thousands of events occurring between 24 April and 21 May (Figure 3) [*Wilcock et al*., 2016]. The signals are similar in character to those reported by *Schlindwein et al*. [2005] using seismic sensors deployed on an ice flow near a submarine volcano along the Gakkel Ridge, and by *Tan et al*. [2016] in association with ocean bottom seismic observations from the 2006 eruption at 9°50′N on the East Pacific Rise.

Explosions from the north rift have several arrivals, as shown in Figures 4–6. Modeling suggests that none of these arrivals is a direct path; even the first pulse most likely reflected at least once prior to its arrival at the caldera stations and thus is inverted from its original orientation. Each subsequent pulse has undergone

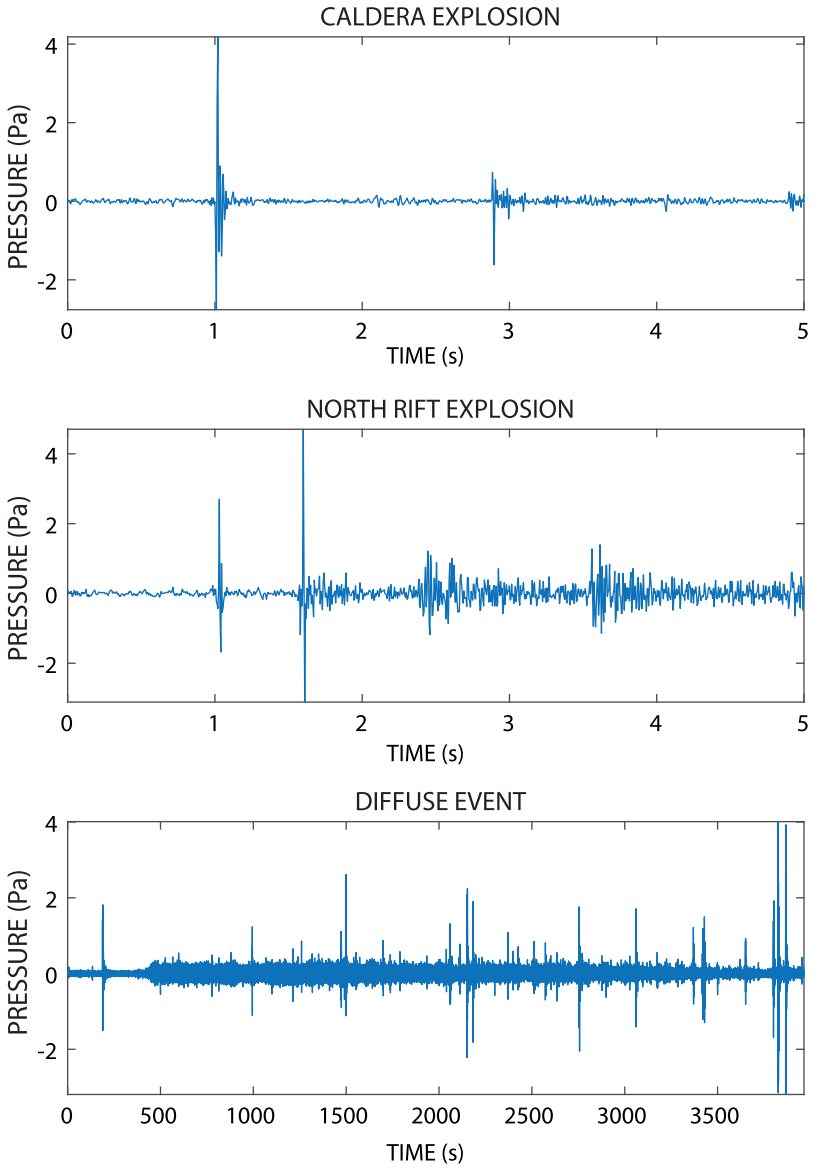

Figure 5. Acoustic records of the three types of explosive signals, as recorded by the hydrophone at AXCC1. The caldera event has 1 weak surface reflection ~1.8 s after the first arrival whereas the north rift event has several reflected arrivals. The diffuse explosion is represented by the weak (<0.5 Pa) signal beginning at ~500 s. The short duration high amplitude pulses are north rift explosions that may or may not be associated with the diffuse event.

more reflections off of the sea surface and/or seafloor, each of which affects the shape of the waveform. In many cases, the secondary arrival for north rift explosions has greater amplitude than the primary arrival (Figure 6). This, combined with the more complex nature of the second pulse, may be due to interference of simultaneous arrivals. The relative amplitudes of the first three arrivals vary by location, at least in a broad sense; caldera explosions have weak secondary arrivals and no clear arrivals after that, whereas explosions on the north rift exhibit at least three strong arrivals, with additional weaker, and more extended arrivals after that (Figure 5). The range of amplitudes may reflect variation in reflected energy, as acoustic waves likely hit the sea surface at different angles, and reflection coefficients are highly dependent on the angle of incidence.

Among the north rift explosions, many events exhibit waveform similarity, suggestive of a repeating source process (Figures 6 and 7). Multiplets were therefore identified based on similarity across the first two arrivals, as later arrivals are likely affected by subtle differences in reflection locations, and the effects of

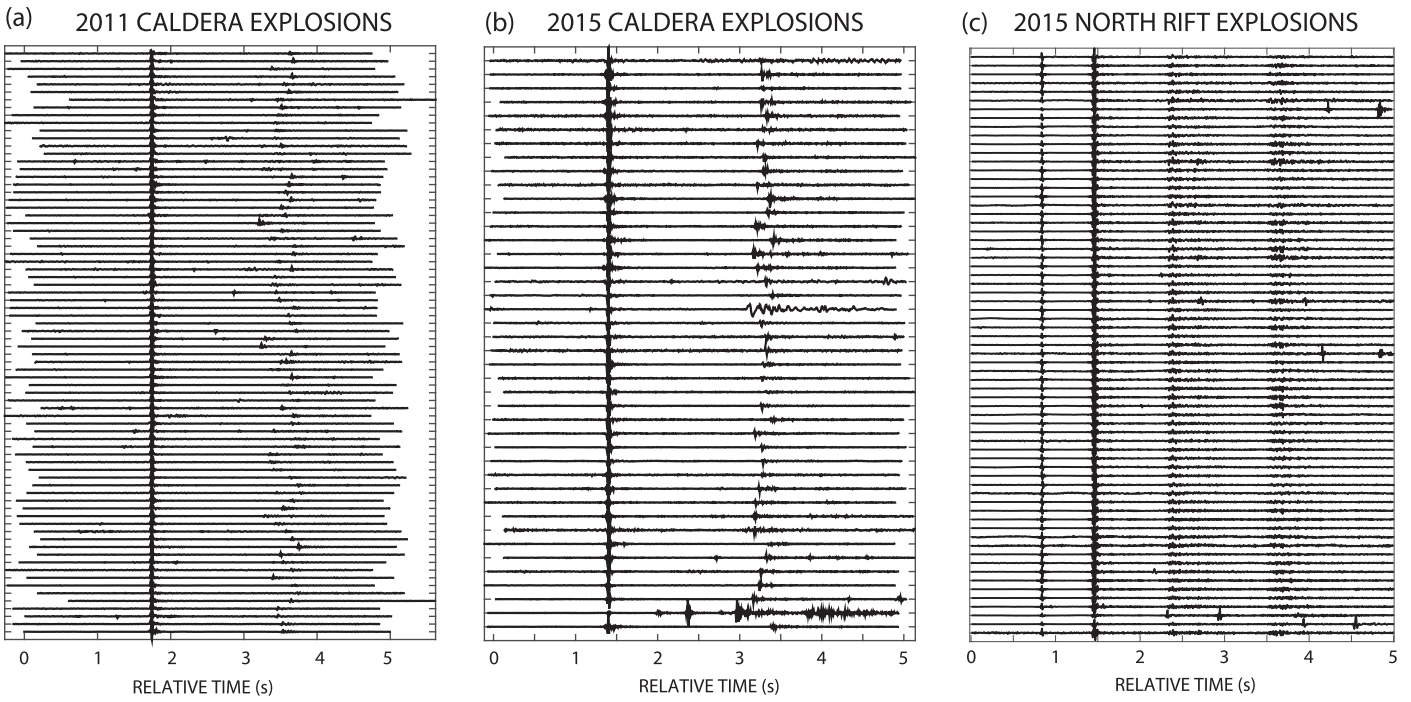

Figure 6. Three explosion multiplets. (a) Caldera explosions during the 2011 eruption, as recorded by OBHN, (b) caldera explosions during the 2015 eruption, as recorded at station AXCC1 on channel HDH (the hydrophone), (c) north rift explosions during the 2015 eruption, as recorded by station AXCC1 on channel HDH. Secondary arrivals caused by sea surface reflections are visible ~1.5–2 s after the first arrival for the caldera events. Variability in the timing of the reflected arrival is due to variation in source location. The secondary arrival for the north rift explosions occurs ~0.6 s after the first arrival, with later phases resulting from additional seafloor or sea surface reflections.

multipathing. Multiplets are generally considered to share a common source process and to have their origin within a quarter wavelength of one another [*Geller and Mueller*, 1980]. The high-frequency (50–100 Hz) nature of the explosions therefore suggests that the source location for each multiplet is a region of no more than 8 m in diameter.

A data set of >30,000 explosion events was used for multiplet analysis; all events were cross-correlated and clustered by similarity (with a correlation threshold of 0.8). The 10 largest multiplets are displayed in Figure 8, alongside the dates when these events were recorded. The first four arrivals for most multiplets are shown, with the exception of cluster 5, a subset of the caldera explosions, which has a single reflected arrival. Clusters 4 and 8 overlap in time with the caldera explosions, while most of the other multiplets took place in the several days that followed. Cluster 10 took place well after the other multiplets and exhibits slightly different reflection timing, indicative of a small change in source location.

6.3. Ash-Producing Eruption Signals

The final category of acoustic signals in the eruption is a diffuse, prolonged, broadband (0–100 Hz) signal (Figure 9). The prolonged nature of the diffuse signals distinguishes them from other explosion signals observed at Axial. Durations are approximate, as the signal fades into noise, but the events range from ~2 min to ~1 h. This signal is only weakly recorded by the seismometers of the OOI, suggesting that it does not couple strongly from the water column into the ground. The first such event was recorded on 1 May, coincident with the decline of earthquake activity at Axial (Figure 1), and with a shift in character of the explosion multiplets (Figure 7b). A total of 45 diffuse events were recorded between 1 and 20 May.

Unlike the discrete explosion signals that locate within the caldera and on Axial's north rift, the diffuse signals cannot easily be located. Their onsets are emergent, and they are only weakly recorded on seismic channels. However, a comparison of their envelopes suggests that the signals arrive nearly simultaneously at stations AXCC1 and AXEC2, but arrive significantly later (10–15 s) at AXBA1, consistent with a location within or to the north of the caldera.

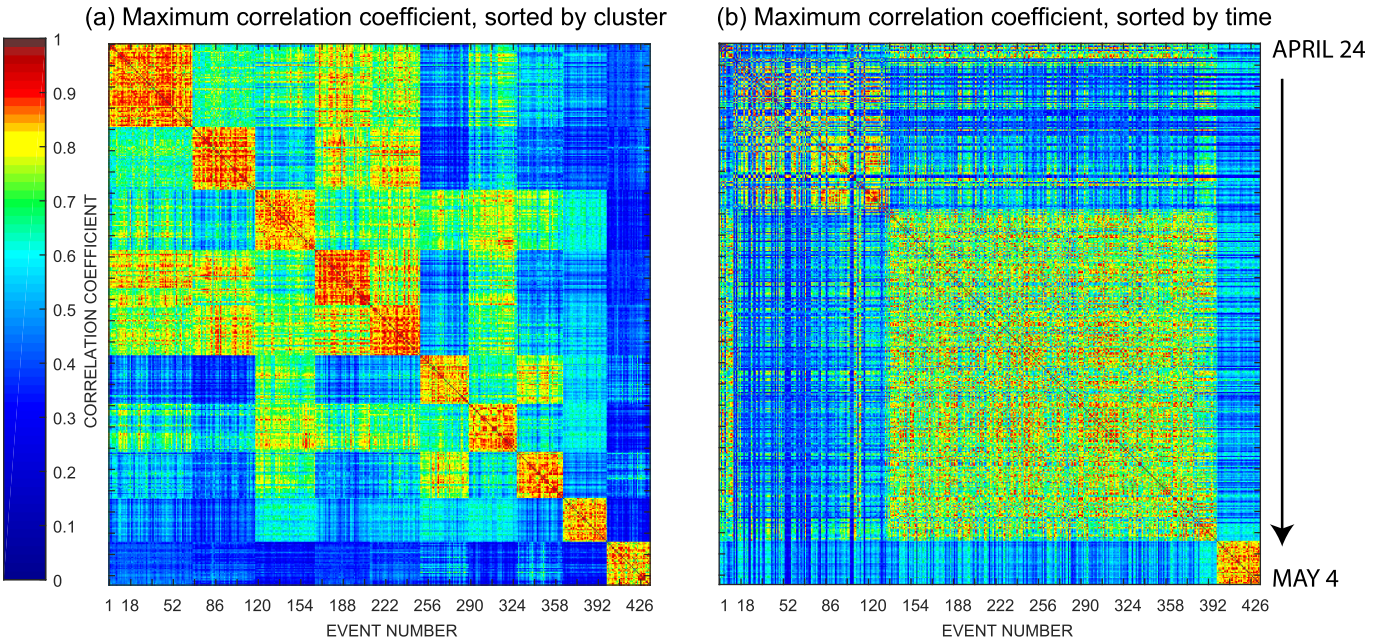

Figure 7. Correlation coefficients for the 10 largest multiplets recorded during the 2015 eruption, sorted by (a) cluster and (b) time. Each multiplet has 30–70 events within it. When sorted by time, the multiplets create larger clusters that, while less similar, suggest broad similarity in source type or location. The final cluster in Figure 7b represents events with slightly different reflection timing, such as those shown in cluster #10 in Figure 8.

That the diffuse broadband signals are associated with an eruptive process is supported by a number of observations. First, no signals of this type were observed either prior to the eruption or after 20 May, suggesting an association with magmatic activity at Axial. Neither ash deposits nor the diffuse hydroacoustic signal were observed during the 2011 eruption. Second, and perhaps most intriguingly, the diffuse broadband signals bear strong resemblance to hydroacoustic signals recorded in association with magmatic degassing and tephra production at two other submarine volcanoes: NW Rota-1 in the Marianas arc [*Chadwick et al*., 2008] and West Mata volcano in the Lau Basin [*Resing et al*., 2011; *Dziak et al*., 2015]. At each of these volcanoes, video and hydrophone data show that ash effusion at the vent was accompanied by pulses of broadband (0–100 Hz) noise lasting tens of seconds to minutes. The duration of explosive bursts at Axial, as inferred from the hydroacoustic data, is substantially longer, ranging from 2 to 60 min (Figure 7).

Water temperatures, as recorded on the Axial instruments, were observed to rise during the eruption (Figure 10). The greatest increase in temperature occurred following the decline in the numbers of both earthquakes and north rift explosions. Water temperature measured at AXCC1, however, correlates well with the cumulative duration of diffuse activity (Figure 10). As the diffuse events cease, the water temperature falls. Although this correlation cannot definitively be shown to be causal, it is consistent with a model in which prolonged explosive activity releases heat into the water in the caldera region.

7. Eruption Sequence

On ROV dives on Axial volcano in August 2015, eruption products were found in four places: (1) lava flows in the northeastern caldera, (2) on the northeastern caldera rim, (3) on the north rift zone, and (4) fine ash deposits on multiple benchmarks in the central and southern caldera [*Chadwick et al*., 2016]. Analysis of the ash shows that it is chemically similar to the NE caldera lava flows and the flows on the caldera rim, both of which are mafic end-members among Axial lavas erupted over the past several hundred years [*Chadwick et al*., 2016].

Relative to other explosions recorded during the 2015 eruption, the caldera explosions are weak and short-lived. Although both explosion types have similar amplitude at station AXCC1 (∼5 Pa; Figure 5), the caldera events are <5 km from the station while the north rift events are ∼15–20 km away. Furthermore, the first

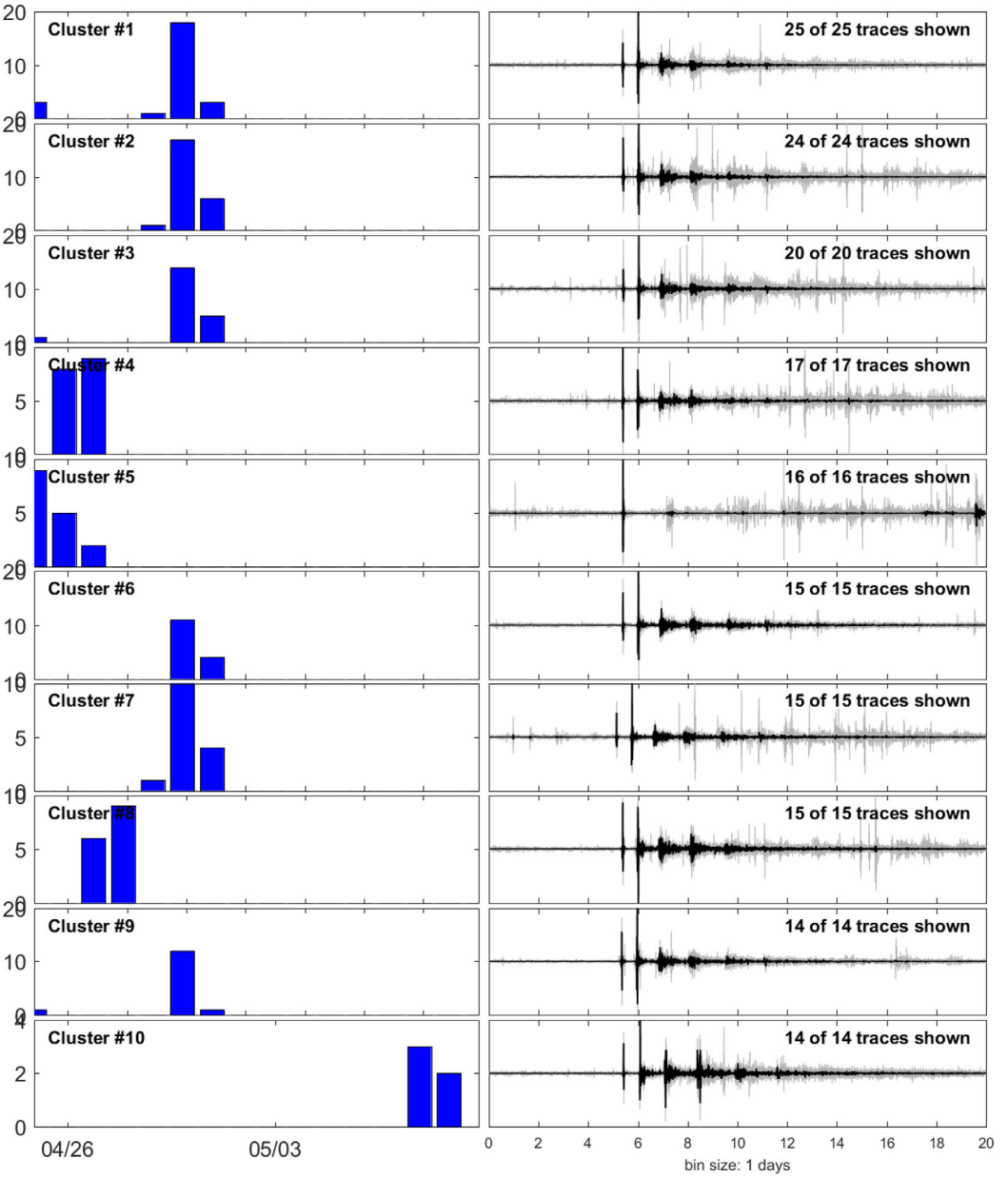

Figure 8. Occurrence histogram for explosion multiplets recorded during the 2015 eruption. Cluster #5, which occurs first among the events, is a multiplet of caldera explosions, while most others locate to the north. The last multiplet, cluster #10 occurs latest in the eruption. The timing between first and second arrivals for cluster #10 is slightly longer than that of the other north rift multiplets, suggesting a different source location.

arriving signals from the north rift likely lose energy upon reflection from the water surface, so their original amplitudes were likely significantly larger. The greater energy of the north rift explosions relative to those in the caldera is not yet fully understood but may be related to differences in gas pressure or lava viscosity. The caldera explosions are observed only for the first few days of the eruption whereas the north rift events endure for several weeks. This is consistent with observations made by *Chadwick et al*. [2016] suggesting that the caldera lava flow was emplaced rapidly and cooled quickly, while the northern lava flows erupted over a longer time period.

Imagery from the ROV dives reveals that the 2015 lava flows have a significant number of explosion pits, interpreted as steam blasts that ruptured the surface of the flow [*Chadwick et al*., 2016]. It is likely that the formation of these pits generates a significant impulsive acoustic signal, and both *Wilcock et al*. [2016] and *Chadwick et al*. [2016] have proposed that they are the source of the explosion signals. However, the

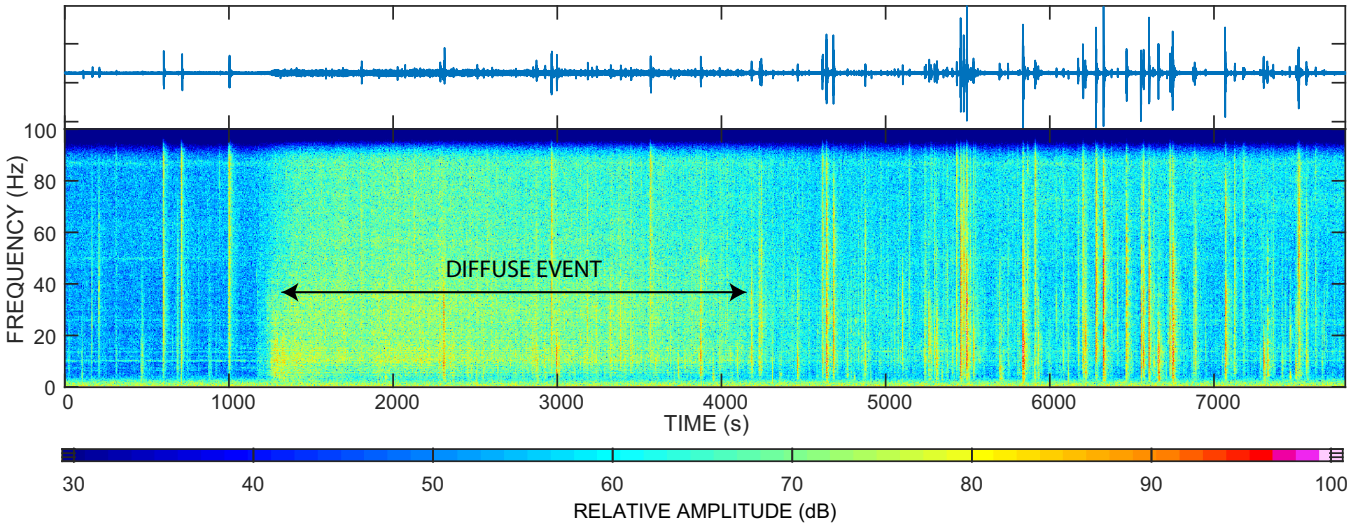

Figure 9. Diffuse broadband event, 2 May, as recorded by the hydrophone at station AXCC1. Forty-five such events were recorded between 1 and 20 May 2015. Such broadband events bear similarity to hydroacoustic signals recorded in association with explosive degassing at NW Rota-1 and West Mata submarine volcanoes.

repetitive nature of the explosion signals suggests a nondestructive source, or at least one that can repeat multiple times within a restricted area. The correlogram in Figure 8a shows that multiplets occur in relatively small (20–50 event) clusters, so no one region or source produces more than a few dozen explosions. Most of the explosion signals likely reflect small steam bursts that fragment the outer portion of the lava flow, as these events can repeat in a small region. In contrast, destructive processes such as the formation of collapse pits would be nonrepeating and unlikely to produce multiplets.

A subset of explosion multiplets, plotted according to cluster (similar events plot next to one another), are shown in Figure 7a. However, when the events are plotted according to when they occurred (Figure 7b), it is clear that there are broader correlations that change as a function of time, potentially reflecting eruption from different regions of the lava flows. We identify at least four distinct time periods: 24–25 April, 25–28 April, 28 April to 1 May, and 1–12 May. Multiplet events recorded from 25–28 April are distinct from the other broad clusters, while those occurring between 24–25 April, and 28 April and 1 May are somewhat alike. A change in eruption location within the north lava flows could well explain these different clusters. Explosions occurring after 1 May do not correlate well with any of the other multiplets, and the 1–12 May cluster shows a subtle difference in the timing of the first several pulses: the first two pulses, as recorded on station AXCC1, occur 0.60 s apart prior to 1 May, and 0.66 s apart after that time, again suggestive of a subtle change in source location. Many events occurring after 1 May locate near the southernmost of the two largest north lava flows, supporting this model (Figure 1).

The first of the diffuse broadband signals was also recorded on 1 May, well after the eruption initiated on 24 April. Although it is plausible that other such events occurred in the first few hours of the eruption, when

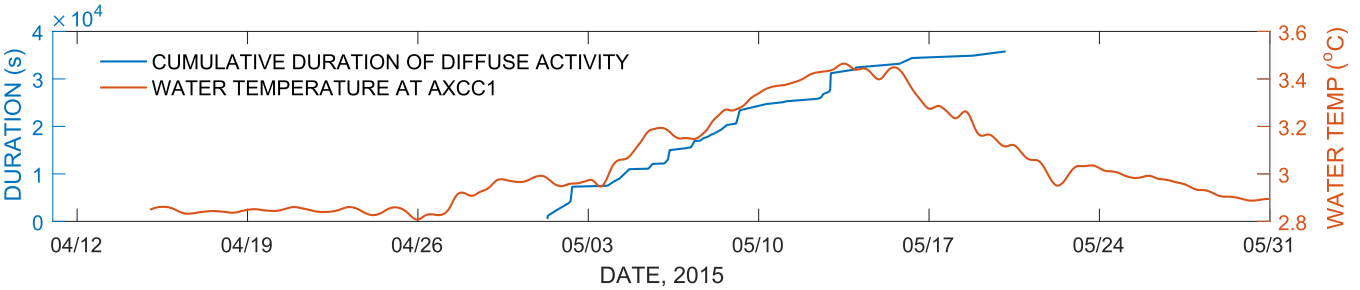

Figure 10. Water temperature recorded at station AXCC1 (red) and cumulative duration of diffuse activity (blue). Water temperatures rose following the beginning of the eruption (April 24) and remained relatively constant over the next week. A significant increase in water temperature on 3 May coincides with the onset of diffuse activity, interpreted here as explosive, ash-producing eruptions. This may reflect the addition of heat to the water in the caldera during Hawaiian-style explosive activity.

instruments were saturated by near-continuous seismic and explosion activity, there is no clear evidence of diffuse events early in the eruption sequence.

We propose that the diffuse broadband signals recorded during the waning phases of the Axial eruption represent submarine Hawaiian eruptions that generated pyroclastic material, akin to subaerial fire fountaining. These signals may also have been the source of fine, glassy, ash shards collected in the central Axial caldera following the eruption [*Clague et al*., 2009; *Chadwick et al*., 2016], although vigorous degassing without pyroclast formation could also generate hydroacoustic noise. If in fact the ash was produced in one of the diffuse episodes, this model implies that the volcano underwent a shift from purely effusive activity in the first week of the eruption, to more explosive activity as seismic activity waned. Even if the diffuse events result from gas, and not ash, ejection, they still reveal a change in eruption products from gas-poor to gas-rich.

Head and Wilson [2003] describe a variety of mechanisms by which explosive activity may occur in the deep submarine environment, including via Hawaiian, Strombolian, and Vulcanian explosions. The Vulcanian model is compelling at Axial in that it describes the rapid ejection of gas trapped beneath a lava flow, consistent with the relative timing of lava and pyroclastic production at Axial. Vulcanian eruptions, however, would be expected to generate significant and impulsive seismic and acoustic signals as the lava cap is fractured prior to gas ejection [*Vergniolle and Caplan-Auerbach*, 2006; *Caplan-Auerbach et al*., 2010]. Strombolian explosions are caused by slug flow and may generate impulsive explosion signals [e.g., *Schlindwein and Riedel*, 2010] rather than the prolonged sounds recorded here. Furthermore, both Strombolian and Vulcanian activity would be expected to generate mostly large eruptive blocks, with fine sediment deposited close to the vent [*Head and Wilson*, 2003]. In the case of the Axial eruption, extremely fine ash was observed within the caldera, hundreds of meters from the caldera lava flow. This requires an eruption mechanism that fragments the magma and generates an eruptive plume that can be carried away from the source. Given that an increase in temperature was observed at the same time, it is plausible that the ash was transported by a warm eruption plume. Both of these models are consistent with *Head and Wilson*'s [2003] description of submarine Hawaiian activity formed by collection of a foam in a magma reservoir.

We propose that eruption of the caldera and north rift lavas at Axial allowed deeper magma within the reservoir to decompress, exsolving gas that collected below the reservoir roof. The resulting Hawaiian release of volatiles was accompanied by diffuse, broadband hydroacoustic signals, and a thermal plume that distributed fine ash within the caldera. The data presented in Figure 2 show that the Hawaiian explosions initiated on 1 May, just as the number of earthquakes reached a minimum, and while the north rift explosions were on the decline. The lack of caldera seismicity suggests that earlier eruptive activity may have opened pathways to the seafloor, allowing later gas release to occur aseismically.

The transition to gas-rich activity took place near the beginning of May. Several days after the first diffuse events were recorded on 1 May, bottom pressure recorders (BPRs) indicate that rapid deflation slowed [*Nooner and Chadwick*, 2016]. The BPRs show some variability over the next few weeks, but all show that deflation ended on 19 May, coincident with the termination of diffuse activity, as detected by the hydrophones. We propose that this represents the end of the eruption.

8. Conclusions

The hydroacoustic data presented here are the first to span an eruptive sequence at a submarine volcano, and the first to distinguish three types of explosive signals. The long-term record shows that while inflation began immediately after the 2011 eruption [*Nooner and Chadwick*, 2016], seismic evidence of reservoir recharge began in early 2013, less than 2 years after the end of the 2011 eruption. Rapid inflation of the magma reservoir [*Nooner and Chadwick*, 2016] resulted in eruption just over 2 years later. The seismic quiescence observed after the 2015 eruption is similar to that recorded following the 2011 event (Figure 2), and after the 1998 eruption [*Sohn et al*., 2004].

The hydroacoustic data support the model put forth by *Wilcock et al*. [2016] that the 2015 eruption began as a lava flow within the caldera, accompanied by explosions at the lava water interface. Shortly after the eruption began, it transitioned to the north rift, where voluminous lava flows erupted for several weeks, also creating explosions with associated hydroacoustic signals. The initial eruption of magmas reduced the

pressure within the magma chamber, allowing the formation of foam and the subsequent eruption of volatiles through fractures connecting the reservoir to the surface, either within the caldera or to the north. Beginning on 1 May, these degassing events generated ash through a series of Hawaiian explosions. This was the final phase of the eruption, which ended near 20 May, almost a month after its initiation.

The presence of real-time hydrophones on the seafloor during the 2015 eruption provided a means by which different explosion types could be identified. The three types of events, small caldera explosions, strong explosions in the north rift, and diffuse signals associated with explosive degassing, provide insight into the dynamics of an eruption that was otherwise hidden from view. Previous work suggests that the impulsive signals presented here are not unique to the Axial system [*Schlindwein et al*., 2005; *Tan et al*., 2016], suggesting that hydroacoustic data may be an important tool in tracking the distribution and timing of lava flows in the deep-sea. Notably, the Hawaiian degassing events were identifiable primarily through hydroacoustic data, as they only weakly couple into the ground where seismometers can detect them. These diffuse events have previously been identified only at submarine arc volcanoes, and their presence at Axial supports arguments by *Head and Wilson* [2003] and *Clague et al*. [2009] that this type of explosive submarine eruptive activity may be more common than has been previously appreciated. Because these events couple poorly into the ground, hydroacoustic data may be the best means by which such eruptions can be identified at other submarine volcanoes.

Acknowledgments

We are grateful to M. Tolstoy and an anonymous reviewer for comments that greatly improved the manuscript. Thanks to W. W. Chadwick, D. Clague, M. E. Mann, and W. Wilcock for helpful discussions and comments. OOI hydrophone data are available through the IRIS Data Management Center. NOAA OBH data are available upon e-mail request to the authors (caplanj@wwu.edu). D.R.B. was supported by NSF OCE-1635276. C.G. was supported by NSF DGE-1256082. This paper is NOAA-PMEL contribution number 4594.

References

Caplan-Auerbach, J., A. K. Bellesiles, and J. J. Fernandes (2010), Estimates of eruption velocity and plume height from infrasonic recordings of the 2006 eruption of Augustine Volcano, Alaska, *J. Volcanol. Geotherm. Res.*, *189*(1–2), 12–18.

Caress, D. W., D. A. Clague, J. B. Paduan, J. F. Martin, B. M. Dreyer, W. W. Chadwick Jr, A. Denny, and D. S. Kelley (2012), Repeat bathymetric surveys at 1-metre resolution of lava flows erupted at Axial Seamount in April 2011, *Nat. Geosci.*, *5*(7), 483–488.

Chadwick, W. W., S. L. Nooner, M. A. Zumberge, R. W. Embley, and C. G. Fox (2006), Vertical deformation monitoring at Axial Seamount since its 1998 eruption using deep-sea pressure sensors, *J. Volcanol. Geotherm. Res.*, *150*(1), 313–327.

Chadwick, W. W., K. V. Cashman, R. W. Embley, H. Matsumoto, R. P. Dziak, C. E. J. De Ronde, T.-K. Lau, N. D. Deardorff, and S. G. Merle (2008), Direct video and hydrophone observations of submarine explosive eruptions at NW Rota-1 volcano, Mariana arc, *J. Geophys. Res.*, *113*, B08S10, doi:10.1029/2007JB005215.

Chadwick, W. W., S. L. Nooner, D. A. Butterfield, and M. D. Lilley (2012), Seafloor deformation and forecasts of the April 2011 eruption at Axial Seamount, *Nat. Geosci.*, *5*(7), 474–477.

Chadwick, W. W., J. B. Paduan, D. A. Clague, B. M. Dreyer, S. G. Merle, A. M. Bobbitt, D. W. Caress, B. Philip, D. S. Kelley, and S. L. Nooner (2016), Voluminous eruption from a zoned magma body after an increase in supply rate at Axial Seamount, *Geophys. Res. Lett.*, *43*, 12,063–12,070, doi:10.1002/2016GL071327.

Clague, D. A., J. B. Paduan, and A. S. Davis (2009), Widespread Strombolian eruptions of mid-ocean ridge basalt, *J. Volcanol. Geotherm. Res.*, *180*, 171–188.

Clague, D. A., et al. (2013), Geologic history of the summit of Axial Seamount, Juan de Fuca Ridge, *Geochem. Geophys. Geosyst.*, *14*, 4403–4443, doi:10.1002/ggge.20240.

Dziak, R. P., and C. G. Fox (1999), Long-term seismicity and ground deformation at Axial Volcano, Juan de Fuca Ridge, *Geophys. Res. Lett.*, *26*(24), 3641–3644.

Dziak, R. P., J. H. Haxel, D. R. Bohnenstiehl, W. W. Chadwick Jr., S. L. Nooner, M. J. Fowler, H. Matsumoto, and D. A. Butterfield (2012), Seismic precursors and magma ascent before the April 2011 eruption at Axial Seamount, *Nat. Geosci.*, *5*(7), 478–482.

Dziak, R. P., D. R. Bohnenstiehl, E. T. Baker, H. Matsumoto, J. Caplan-Auerbach, R. W. Embley, S. G. Merle, S. L. Walker, T.-K. Lau, and W. W. Chadwick (2015), Long-term explosive degassing and debris flow activity at West Mata submarine volcano, *Geophys. Res. Lett.*, *42*, 1480–1487, doi:10.1002/2014GL062603.

Embley, R. W., K. M. Murphy, and C. G. Fox (1990), High resolution studies of the summit of Axial Volcano, *J. Geophys. Res.*, *95*(B8), 12,785–12,812.

Embley, R. W., et al. (2006), Long-term eruptive activity at a submarine arc volcano, *Nature*, *441*(7092), 494–497.

Fox, C. G. (1999), In situ ground deformation measurements from the summit of Axial Volcano during the 1998 volcanic episode, *Geophys. Res. Lett.*, *26*(23), 3437–3440.

Fox, C. G., and R. P. Dziak (1998), Hydroacoustic detection of volcanic activity on the Gorda Ridge, February–March 1996, *Deep Sea Res., Part II*, *45*, 2513–2530.

Fox, C. G., W. E. Radford, R. P. Dziak, T. K. Lau, H. Matsumoto, and A. E. Schreiner (1995), Acoustic detection of a seafloor spreading episode on the Juan de Fuca Ridge using military hydrophone arrays, *Geophys. Res. Lett.*, *22*(2), 131–134.

Fox, C. G., W. W. Chadwick, and R. W. Embley (2001), Direct observation of a submarine volcanic eruption from a sea-floor instrument caught in a lava flow, *Nature*, *412*(6848), 727–729.

Garcia, C., W. S. D. Wilcock, Y. J. Tan, and M. Tolstoy (2015), Impulsive seafloor signals from the 2015 eruption of axial seamount, Abstract S51D-2711 presented at 2015 Fall Meeting, AGU, San Francisco, Calif., 14–18 Dec.

Geller, R. J., and C. S. Mueller (1980), Four similar earthquakes in central California, *Geophys. Res. Lett.*, *7*(10), 821–824.

Head, J. W., III, and L. Wilson (2003), Deep submarine pyroclastic eruptions: Theory and predicted landforms and deposits, *J. Volcanol. Geotherm. Res.*, *121*, 155–193.

Hoffe, B. H., P. W. Cary, and L. R. Lines (1999), A simple and robust method for combining dual-sensor OBC data?, CREWES Research report, vol. 11. [Available at http://crewes.org/ForOurSponsors/ResearchReports/1999/1999-24.pdf.]

Kelley, D. S., J. R. Delaney, and S. K. Juniper (2014), Establishing a new era of submarine volcanic observatories: Cabling Axial Seamount and the Endeavour Segment of the Juan de Fuca Ridge, *Mar. Geol.*, *352*, 426–450.

Mellinger, D. K. (2001), ISHMAEL 1.0 user's guide, *NOAA Tech. Memo. OAR-PMEL-120*, 30 p., NOAA PMEL, Seattle, Wash.
Müller, C., and W. Jokat (2000), Seismic evidence for volcanic activity discovered in Central Arctic, *Eos Trans. AGU*, *81*(24), 265.
Nooner, S. L., and W. W. Chadwick Jr. (2009), Volcanic inflation measured in the caldera of Axial Seamount: Implications for magma supply and future eruptions, *Geochem. Geophys. Geosyst.*, *10*, Q02002, doi:10.1029/2008GC002315.
Nooner, S. L., and W. W. Chadwick (2016), Inflation-predictable behavior and co-eruption deformation captured by cabled instruments at Axial Seamount, *Science*, *354*(6318), 1399–1403.
Resing, J. A., et al. (2011), Active submarine eruption of boninite in the northeastern Lau Basin, *Nat. Geosci.*, *4*(11), 799–806.
Rubin, K. H., S. A. Soule, W. W. Chadwick Jr., D. J. Fornari, D. A. Clague, R. W. Embley, E. T. Baker, M. R. Perfit, D. W. Caress, and R. P. Dziak (2012), Volcanic eruptions in the deep sea, *Oceanography*, *25*(1), 142–157.
Schlindwein, V., and C. Riedel (2010), Location and source mechanism of sound signals at Gakkel Ridge, Arctic Ocean: Submarine Strombolian activity in the 1999-2001 volcanic episode, *Geochem. Geophys. Geosyst.*, *11*, Q01002, doi:10.1029/2009GC002706.
Schlindwein, V., C. Müller, and W. Jokat (2005), Seismoacoustic evidence for volcanic activity on the ultraslow-spreading Gakkel Ridge, Arctic Ocean, *Geophys. Res. Lett.*, *32*, L18306, doi:10.1029/2005GL023767.
Sohn, R. A., W. C. Crawford, and S. C. Webb (1999), Local seismicity following the 1998 eruption of Axial Volcano, *Geophys. Res. Lett.*, *26*(23), 3433–3436.
Sohn, R. A., A. H. Barclay, and S. C. Webb (2004), Microearthquake patterns following the 1998 eruption of Axial Volcano, Juan de Fuca Ridge: Mechanical relaxation and thermal strain, *J. Geophys. Res. Solid Earth*, *109*(B1).
Tan, Y. J., M. Tolstoy, F. Waldhauser, and W. S. D. Wilcock (2016), Plate boundary unzipped: Dynamics of a seafloor spreading episode at the East Pacific Rise, *Nature*, *540*, 261–265.
Thorwart, M., and T. Dahm (2005), Wavefield decomposition for passive ocean bottom seismological data, *Geophys. J. Int.*, *163*, 611–621, doi:10.1111/j.1365-246X.2005.02761.x.
Tolstoy, M., D. R. Bohnenstiehl, M. H. Edwards, and G. J. Kurras (2001), Seismic character of volcanic activity at the ultraslow-spreading Gakkel Ridge, *Geology*, *29*, 1139–1142.
Tolstoy, M., et al. (2006), A sea-floor spreading event captured by seismometers, *Science*, *314*(5807), 1920–1922.
Vergniolle, S., and J. Caplan-Auerbach (2006), Basaltic Subplinian plumes and thermals: Constraints from acoustic measurements at Shishaldin volcano, Alaska, *Bull. Volcanol.*, *68*, 611–630.
Wilcock, W. S. D., M. Tolstoy, F. Waldhauser, C. Garcia, Y. Joe Tan, D. R. Bohnenstiehl, J. Caplan-Auerbach, R. P. Dziak, A. F. Arnulf, and M. E. Mann (2016), The 2015 eruption of Axial Seamount: Seismic constraints on caldera dynamics, *Science*, *354*(6318), 1395–1399.